Measurement of ϕ_3 with a Dalitz plot analysis of $B^+ \to D^{(*)}K^{(*)+}$ decay

A. Poluektov,[1] K. Abe,[6] K. Abe,[43] I. Adachi,[6] H. Aihara,[45] D. Anipko,[1] K. Arinstein,[1] T. Aushev,[11] S. Bahinipati,[4] A. M. Bakich,[40] V. Balagura,[11] E. Barberio,[19] M. Barbero,[5] I. Bedny,[1] K. Belous,[10] U. Bitenc,[12] I. Bizjak,[12] S. Blyth,[22] A. Bondar,[1] A. Bozek,[25] M. Bračko,[6,18,12] T. E. Browder,[5] P. Chang,[24] Y. Chao,[24] A. Chen,[22] W. T. Chen,[22] B. G. Cheon,[3] R. Chistov,[11] Y. Choi,[39] A. Chuvikov,[33] J. Dalseno,[19] M. Danilov,[11] M. Dash,[49] A. Drutskoy,[4] S. Eidelman,[1] D. Epifanov,[1] S. Fratina,[12] N. Gabyshev,[1] A. Garmash,[33] T. Gershon,[6] G. Gokhroo,[41] B. Golob,[17,12] A. Gorišek,[12] J. Haba,[6] T. Hara,[30] K. Hayasaka,[20] H. Hayashii,[21] M. Hazumi,[6] T. Hokuue,[20] Y. Hoshi,[43] W.-S. Hou,[24] T. Iijima,[20] K. Ikado,[20] K. Inami,[20] A. Ishikawa,[45] H. Ishino,[46] R. Itoh,[6] Y. Iwasaki,[6] H. Kawai,[2] T. Kawasaki,[27] H. R. Khan,[46] H. J. Kim,[15] K. Kinoshita,[4] S. Korpar,[18,12] P. Križan,[17,12] P. Krokovny,[1] R. Kulasiri,[4] R. Kumar,[31] C. C. Kuo,[22] A. Kuzmin,[1] Y.-J. Kwon,[50] J. Lee,[37] T. Lesiak,[25] J. Li,[36] D. Liventsev,[11] J. MacNaughton,[9] G. Majumder,[41] F. Mandl,[9] D. Marlow,[33] T. Matsumoto,[47] A. Matyja,[25] S. McOnie,[40] W. Mitaroff,[9] K. Miyabayashi,[21] H. Miyake,[30] H. Miyata,[27] D. Mohapatra,[49] T. Nagamine,[44] I. Nakamura,[6] E. Nakano,[29] Z. Natkaniec,[25] S. Nishida,[6] O. Nitoh,[48] S. Noguchi,[21] T. Nozaki,[6] S. Ogawa,[42] T. Ohshima,[20] S. Okuno,[13] S. L. Olsen,[5] Y. Onuki,[27] H. Ozaki,[6] P. Pakhlov,[11] H. Park,[15] L. S. Peak,[40] R. Pestotnik,[12] L. E. Piilonen,[49] Y. Sakai,[6] T. R. Sarangi,[6] N. Sato,[20] N. Satoyama,[38] K. Sayeed,[4] T. Schietinger,[16] O. Schneider,[16] A. J. Schwartz,[4] R. Seidl,[7,34] M. E. Sevior,[19] M. Shapkin,[10] H. Shibuya,[42] B. Shwartz,[1] J. B. Singh,[31] A. Sokolov,[10] A. Somov,[4] R. Stamen,[6] S. Stanič,[28] M. Starič,[12] H. Stoeck,[40] K. Sumisawa,[30] S. Suzuki,[35] S. Y. Suzuki,[6] F. Takasaki,[6] M. Tanaka,[6] Y. Teramoto,[29] X. C. Tian,[32] K. Trabelsi,[5] T. Tsukamoto,[6] S. Uehara,[6] T. Uglov,[11] K. Ueno,[24] Y. Unno,[6] S. Uno,[6] P. Urquijo,[19] Y. Ushiroda,[6] Y. Usov,[1] G. Varner,[5] K. E. Varvell,[40] S. Villa,[16] C. H. Wang,[23] Y. Watanabe,[46] E. Won,[14] Q. L. Xie,[8] B. D. Yabsley,[40] A. Yamaguchi,[44] Y. Yamashita,[26] M. Yamauchi,[6] J. Ying,[32] L. M. Zhang,[36] Z. P. Zhang,[36] V. Zhilich,[1] and D. Zürcher[16]

(Belle Collaboration)

[1]*Budker Institute of Nuclear Physics, Novosibirsk*
[2]*Chiba University, Chiba*
[3]*Chonnam National University, Kwangju*
[4]*University of Cincinnati, Cincinnati, Ohio 45221*
[5]*University of Hawaii, Honolulu, Hawaii 96822*
[6]*High Energy Accelerator Research Organization (KEK), Tsukuba*
[7]*University of Illinois at Urbana-Champaign, Urbana, Illinois 61801*
[8]*Institute of High Energy Physics, Chinese Academy of Sciences, Beijing*
[9]*Institute of High Energy Physics, Vienna*
[10]*Institute of High Energy Physics, Protvino*
[11]*Institute for Theoretical and Experimental Physics, Moscow*
[12]*J. Stefan Institute, Ljubljana*
[13]*Kanagawa University, Yokohama*
[14]*Korea University, Seoul*
[15]*Kyungpook National University, Taegu*
[16]*Swiss Federal Institute of Technology of Lausanne, EPFL, Lausanne*
[17]*University of Ljubljana, Ljubljana*
[18]*University of Maribor, Maribor*
[19]*University of Melbourne, Victoria*
[20]*Nagoya University, Nagoya*
[21]*Nara Women's University, Nara*
[22]*National Central University, Chung-li*
[23]*National United University, Miao Li*
[24]*Department of Physics, National Taiwan University, Taipei*
[25]*H. Niewodniczanski Institute of Nuclear Physics, Krakow*
[26]*Nippon Dental University, Niigata*
[27]*Niigata University, Niigata*
[28]*Nova Gorica Polytechnic, Nova Gorica*
[29]*Osaka City University, Osaka*
[30]*Osaka University, Osaka*
[31]*Panjab University, Chandigarh*
[32]*Peking University, Beijing*

[33]*Princeton University, Princeton, New Jersey 08544*
[34]*RIKEN BNL Research Center, Upton, New York 11973*
[35]*Saga University, Saga*
[36]*University of Science and Technology of China, Hefei*
[37]*Seoul National University, Seoul*
[38]*Shinshu University, Nagano*
[39]*Sungkyunkwan University, Suwon*
[40]*University of Sydney, Sydney NSW*
[41]*Tata Institute of Fundamental Research, Bombay*
[42]*Toho University, Funabashi*
[43]*Tohoku Gakuin University, Tagajo*
[44]*Tohoku University, Sendai*
[45]*Department of Physics, University of Tokyo, Tokyo*
[46]*Tokyo Institute of Technology, Tokyo*
[47]*Tokyo Metropolitan University, Tokyo*
[48]*Tokyo University of Agriculture and Technology, Tokyo*
[49]*Virginia Polytechnic Institute and State University, Blacksburg, Virginia 24061*
[50]*Yonsei University, Seoul*
(Received 30 April 2006; published 29 June 2006)

We present a measurement of the unitarity triangle angle ϕ_3 using a Dalitz plot analysis of the $K^0_S\pi^+\pi^-$ decay of the neutral D meson from the $B^\pm \to D^{(*)}K^{(*)\pm}$ process. The method exploits the interference between D^0 and $\bar{D}^0$ to extract the angle ϕ_3, strong phase δ and the ratio r of suppressed and allowed amplitudes. We apply this method to a 357 fb^{-1} data sample collected by the Belle experiment. The analysis uses three modes: $B^+ \to DK^+$, $B^+ \to D^*K^+$ with $D^* \to D\pi^0$, and $B^+ \to DK^{*+}$ with $K^{*+} \to K^0_S\pi^+$, as well as the corresponding charge-conjugate modes. From a combined maximum likelihood fit to the three modes, we obtain $\phi_3 = 53^\circ\,^{+15^\circ}_{-18^\circ}\,(\text{stat}) \pm 3^\circ(\text{syst}) \pm 9^\circ(\text{model})$. The corresponding 2 standard deviation interval is $8^\circ < \phi_3 < 111^\circ$.

DOI: 10.1103/PhysRevD.73.112009 PACS numbers: 12.15.Hh, 13.25.Hw, 14.40.Nd

I. INTRODUCTION

Determinations of the Cabibbo-Kobayashi-Maskawa (CKM) [1] matrix elements provide important checks on the consistency of the standard model and ways to search for new physics. The possibility of observing direct CP violation in $B \to DK$ decays was first discussed by I. Bigi, A. Carter and A. Sanda [2]. Since then, various methods using CP violation in $B \to DK$ decays have been proposed [3–6] to measure the unitarity triangle angle ϕ_3. These methods are based on two key observations: neutral D^0 and $\bar{D}^0$ mesons can decay to a common final state, and the decay $B^+ \to DK^+$ can produce neutral D mesons of both flavors via $\bar{b} \to \bar{c}u\bar{s}$ and $\bar{b} \to \bar{u}c\bar{s}$ transitions, with a relative phase θ_+ between the two interfering amplitudes that is the sum, $\delta + \phi_3$, of strong and weak interaction phases. For the decay $B^- \to DK^-$, the relative phase is $\theta_- = \delta - \phi_3$, so both phases can be extracted from measurements of such charge conjugate B decay modes. However, the use of branching fractions alone requires additional information to obtain ϕ_3. This is provided either by determining the branching fractions of decays to flavor eigenstates (GLW method [3]) or by using different neutral D final states (ADS method [6]).

A Dalitz plot analysis of a three-body final state of the D meson allows one to obtain all the information required for determination of ϕ_3 in a single decay mode. The use of a Dalitz plot analysis for the extraction of ϕ_3 was first discussed by D. Atwood, I. Dunietz and A. Soni, in the context of the ADS method [6]. This technique uses the interference of Cabibbo-favored $D^0 \to K^-\pi^+\pi^0$ and doubly Cabibbo-suppressed $\bar{D}^0 \to K^-\pi^+\pi^0$ decays. However, the small rate for the doubly Cabibbo-suppressed decay limits the sensitivity of this technique.

Three body final states such as $K^0_S\pi^+\pi^-$ [7,8] have been suggested as promising modes for the extraction of ϕ_3. In the Wolfenstein parametrization of the CKM matrix elements, the weak parts of the amplitudes that contribute to the decay $B^+ \to DK^+$ are given by $V^*_{cb}V_{us} \sim A\lambda^3$ (for the $\bar{D}^0K^+$ final state) and $V^*_{ub}V_{cs} \sim A\lambda^3(\rho + i\eta)$ (for D^0K^+). The two amplitudes interfere as the D^0 and $\bar{D}^0$ mesons decay into the same final state $K^0_S\pi^+\pi^-$; we denote the admixed state as $\tilde{D}_+$. Assuming no CP asymmetry in neutral D decays, the amplitude of the $\tilde{D}_+$ decay as a function of Dalitz plot variables $m^2_+ = m^2_{K^0_S\pi^+}$ and $m^2_- = m^2_{K^0_S\pi^-}$ is

$$M_+ = f(m^2_+, m^2_-) + re^{i\phi_3 + i\delta} f(m^2_-, m^2_+), \qquad (1)$$

where $f(m^2_+, m^2_-)$ is the amplitude of the $\bar{D}^0 \to K^0_S\pi^+\pi^-$ decay, and r is the ratio of the magnitudes of the two interfering amplitudes. The value of r is given by the ratio of the CKM matrix elements $|V^*_{ub}V_{cs}|/|V^*_{cb}V_{us}| \sim 0.38$ and the color suppression factor, and is estimated to be in the range 0.1–0.2 [9].

Similarly, the amplitude of the $\tilde{D}_-$ decay from $B^- \to DK^-$ process is

$$M_- = f(m_-^2, m_+^2) + re^{-i\phi_3+i\delta} f(m_+^2, m_-^2). \quad (2)$$

The $\bar{D}^0 \to K_S^0\pi^+\pi^-$ decay amplitude f can be determined from a large sample of flavor-tagged $\bar{D}^0 \to K_S^0\pi^+\pi^-$ decays produced in continuum e^+e^- annihilation. Once f is known, a simultaneous fit of B^+ and B^- data allows the contributions of r, ϕ_3 and δ to be separated. The method has a twofold ambiguity: (ϕ_3, δ) and $(\phi_3 + 180°, \delta + 180°)$ solutions cannot be separated. We always choose the solution with $0 < \phi_3 < 180°$. References [7,10] give a more detailed description of the technique.

The method described above can be applied to other modes as well as $B^+ \to DK^+$ decay and its charge-conjugate mode (charge conjugate states are implied throughout the paper). Excited states of neutral D and K mesons can also be used, although the values of δ and r can differ for these decays. Previously, the Belle collaboration performed analyses using this technique for $B^+ \to DK^+$ and $B^+ \to D^*K^+$ decays [10,11]. The latest result, based on a 253 fb^{-1} data sample, is $\phi_3 = 68° \,^{+14°}_{-15°} \pm 13(\text{syst}) \pm 11(\text{model})$ [11]. The *BABAR* collaboration uses the modes $B^+ \to DK^+$, $B^+ \to D^*K^+$, and $B^+ \to DK^{*+}$ [12,13]; their result based on a 211 fb^{-1} data sample is $\phi_3 = 67° \pm 28° \pm 13°(\text{syst}) \pm 11°(\text{model})$. Belle has also performed a separate analysis using the $B^+ \to DK^{*+}$ mode [14]. In the current paper, we report a measurement of ϕ_3 combining the modes $B^+ \to DK^+$, $B^+ \to D^*K^+$ and $B^+ \to DK^{*+}$, based on a 357 fb^{-1} data sample. This analysis supersedes previous Belle results on ϕ_3 using Dalitz plot analysis of $B^+ \to D^{(*)}K^{(*)+}$ decays.

II. EVENT SELECTION

We use a 357 fb^{-1} data sample, corresponding to 386×10^6 $B\bar{B}$ pairs, collected by the Belle detector. The decay chains $B^+ \to DK^+$, $B^+ \to D^*K^+$ with $D^* \to D\pi^0$ and $B^+ \to DK^{*+}$ with $K^{*+} \to K_S^0\pi^+$ are selected for the analysis; the decays $B^+ \to D\pi^+$, $B^+ \to D^*\pi^+$ with $D^* \to D\pi^0$ and $\bar{B}^0 \to D^{*+}\pi^-$ with $D^{*+} \to D\pi^+$ serve as control samples. The neutral D meson is reconstructed in the $K_S^0\pi^+\pi^-$ final state in all cases. We also select decays of $D^{*-} \to \bar{D}^0\pi^-$ produced via the $e^+e^- \to c\bar{c}$ continuum process as a high-statistics sample to determine the $\bar{D}^0 \to K_S^0\pi^+\pi^-$ decay amplitude.

The Belle detector is described in detail elsewhere [15,16]. It is a large-solid-angle magnetic spectrometer consisting of a silicon vertex detector (SVD), a 50-layer central drift chamber (CDC) for charged particle tracking and specific ionization measurement (dE/dx), an array of aerogel threshold Čerenkov counters (ACC), time-of-flight scintillation counters (TOF), and an array of CsI(Tl) crystals for electromagnetic calorimetry (ECL) located inside a superconducting solenoid coil that provides a 1.5 T magnetic field. An iron flux return located outside the coil is instrumented to detect K_L mesons and identify muons (KLM).

Charged tracks are required to satisfy criteria based on the quality of the track fit and the distance from the interaction point in both longitudinal and transverse planes with respect to the beam axis. To reduce the low momentum combinatorial background we require each track to have a transverse momentum greater than 100 MeV/c. Separation of kaons and pions is accomplished by combining the responses of the ACC and the TOF with the dE/dx measurement from the CDC to form a likelihood $\mathcal{L}(h)$, where h is a pion or a kaon. Charged particles are identified as pions or kaons using the likelihood ratio $\mathcal{R}_{\text{PID}}(h) = \mathcal{L}(h)/(\mathcal{L}(K) + \mathcal{L}(\pi))$. For charged kaon identification, we require $\mathcal{R}_{\text{PID}}(K) > 0.7$. This requirement selects kaons with an efficiency of 80% and pions with an efficiency of 5%.

Photon candidates are required to have ECL energy greater than 30 MeV. Neutral pion candidates are formed from pairs of photons with invariant masses in the range 120 to 150 MeV/c^2, i.e. less than 2 standard deviations from the π^0 mass. The momentum of the candidate is then found using a fit constraining the invariant mass to M_{π^0}.

Neutral kaons are reconstructed from pairs of oppositely charged tracks without any pion PID requirement. We require the invariant mass $M_{\pi\pi}$ to satisfy $|M_{\pi\pi} - M_{K_S^0}| < 10$ MeV/c^2, i.e. less than 4 standard deviations from the nominal K_S^0 mass. We also require the reconstructed vertex distance from the interaction point in the plane transverse to the beam axis to be more than 1 mm. This condition retains 89% of the K_S^0 mesons and rejects 55% of the combinatorial $\pi\pi$ background. The momentum of the K_S^0 candidate is found using a fit constraining $M_{\pi\pi}$ to $M_{K_S^0}$.

A. Selection of $D^{*-} \to \bar{D}^0\pi^-$

To determine the $\bar{D}^0 \to K_S^0\pi^+\pi^-$ decay amplitude we use $D^{*\pm}$ mesons produced via the $e^+e^- \to c\bar{c}$ continuum process. The flavor of the neutral D meson is tagged by the charge of the slow pion (which we denote as π_s) in the decay $D^{*-} \to \bar{D}^0\pi_s^-$.

To select neutral D candidates we require the invariant mass of the $K_S^0\pi^+\pi^-$ system to be within 9 MeV/c^2 of the D^0 mass, M_{D^0}. To select events originating from a D^{*-} decay we impose a requirement on the difference $\Delta M = M_{K_S^0\pi^+\pi^-\pi_s} - M_{K_S^0\pi^+\pi^-}$ of the invariant masses of the D^{*-} and the neutral D candidates: 144.6 MeV/$c^2 < \Delta M <$ 146.4 MeV/c^2. The resolutions of the selection variables are $\sigma(\Delta M) = 0.38$ MeV/c^2 and $\sigma(M_{K_S^0\pi^+\pi^-}) = 5.4$ MeV/c^2. The suppression of the combinatorial background from $B\bar{B}$ events is achieved by requiring the D^{*-} momentum in the center-of-mass (CM) frame to be greater than 2.7 GeV/c.

The number of events that pass all selection criteria is 271 621. To obtain the number of background events in our

sample we fit the ΔM distribution. The background is parametrized with the function $b(\Delta M) \sim (1/\Delta M) \times \sqrt{(\Delta M/m_\pi)^2 - 1}$; the function describing the signal is a combination of two Gaussian peaks with the same mean value. The fit finds $(261.9 \pm 1.1) \times 10^3$ signal events and 8698 ± 77 background events corresponding to a background fraction of 3.2%.

B. Selection of $B^+ \to DK^+$

The selection of B candidates is based on the CM energy difference $\Delta E = \sum E_i - E_{\rm beam}$ and the beam-constrained B meson mass $M_{\rm bc} = \sqrt{E^2_{\rm beam} - (\sum \vec{p}_i)^2}$, where $E_{\rm beam}$ is the CM beam energy, and E_i and $\vec{p}_i$ are the CM energies and momenta of the B candidate decay products. We select events with $M_{\rm bc} > 5.2$ GeV/c^2 and $|\Delta E| < 0.2$ GeV for

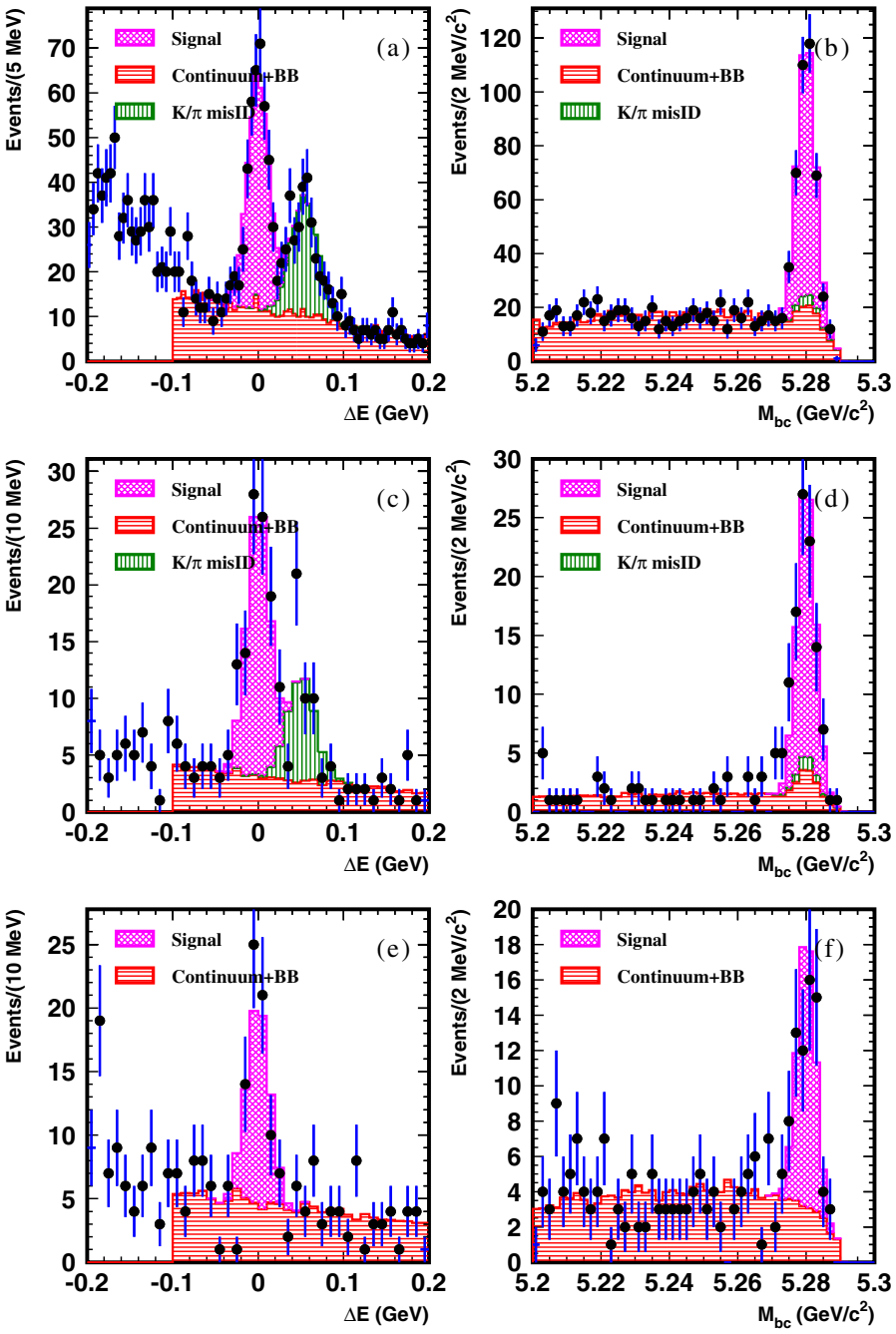

FIG. 1 (color online). ΔE and $M_{\rm bc}$ distributions for the (a,b) $B^+ \to DK^+$, (c,d) $B^+ \to D^*K^+$, and (e,f) $B^+ \to DK^{*+}$ event samples. Points with error bars are the data, and the histogram is the result of a MC simulation according to the fit result. The ΔE distribution is obtained with the signal requirement for $M_{\rm bc}$ (5.27 GeV/$c^2 < M_{\rm bc} <$ 5.3 GeV/c^2); the $M_{\rm bc}$ distribution is obtained with the signal requirement for ΔE ($|\Delta E| < 30$ MeV).

the analysis. In addition, we impose a requirement on the invariant mass of the neutral D candidate: $|M_{K^0_S\pi^+\pi^-} - M_{D^0}| < 11$ MeV/c^2.

To suppress background from $e^+e^- \to q\bar{q}$ ($q = u, d, s, c$) continuum events, we require $|\cos\theta_{\rm thr}| < 0.8$, where $\theta_{\rm thr}$ is the angle between the thrust axis of the B candidate daughters and that of the rest of the event. This requirement retains 80% of the signal and rejects 91% of the continuum background. For additional background rejection, we use a Fisher discriminant composed of 11 parameters [17]: the production angle of the B candidate, the angle of the B thrust axis relative to the beam axis and nine parameters representing the momentum flow in the event relative to the B thrust axis in the CM frame. We apply a requirement on the Fisher discriminant that retains 90% of the signal and rejects 40% of the remaining continuum background.

The ΔE and $M_{\rm bc}$ distributions for $B^+ \to DK^+$ candidates are shown in Fig. 1(a) and 1(b). The peak in the ΔE distribution at $\Delta E = 50$ MeV is due to $B^+ \to D\pi^+$ decays where the pion is misidentified as a kaon. The $B^+ \to DK^+$ selection efficiency (11%) is determined from a Monte Carlo (MC) simulation. The number of events in the signal box ($|\Delta E| < 30$ MeV, 5.27 GeV/$c^2 < M_{\rm bc} <$ 5.3 GeV/c^2) is 470.

For the selected events a two-dimensional unbinned maximum likelihood fit in the variables $M_{\rm bc}$ and ΔE is performed. The resulting signal and background density functions are used in the Dalitz plot fit to obtain the event-by-event signal to background ratio. To parametrize the shape of the $\Delta E - M_{\rm bc}$ distribution, we use two-dimensional Gaussian peaks for the signal contribution and $B^+ \to D\pi^+$ background. The nonpeaking background is parametrized by the sum of two components: the product of an empirical shape introduced by ARGUS [18] as a function of $M_{\rm bc}$ and a linear function in ΔE, and the product of a Gaussian distribution in $M_{\rm bc}$ and a linear function in ΔE. Only the region with $\Delta E > -0.1$ GeV is used in the fit; the region with $\Delta E < -0.1$ GeV includes a large fraction of events from $B \to D^*K$ decay with a lost pion that do not contribute to the signal box. The number of events in the signal peak obtained from the fit is 331 $\pm$ 23; the event purity in the signal box is 67%.

C. Selection of $B^+ \to D^*K^+$

For the selection of $B^+ \to D^*K^+$ events, in addition to the requirements described above, we require that the mass difference $\Delta M = M_{K^0_S\pi^+\pi^-\pi^0} - M_{K^0_S\pi^+\pi^-}$ of neutral D^* and D candidates satisfies 140 MeV/$c^2 < \Delta M <$ 145 MeV/c^2. Figures 1(c) and 1(d) show the ΔE and $M_{\rm bc}$ distributions for $B^+ \to D^*K^+$ candidates. The selection efficiency is 6.2%. The number of events in the signal box is 111. The parametrization of background and signal shapes is the same as that used in the $B^+ \to DK^+$ case. The number of events in the signal peak obtained from the fit is 81 $\pm$ 11; the event purity in the signal box is 77%.

D. Selection of $B^+ \to DK^{*+}$

For $B^+ \to DK^{*+}$ decay candidates, in addition to the requirements placed on the $B^+ \to DK^+$ mode, K^{*+} candidate selection is performed. To select K^{*+} meson candidates, we require the $K^0_S\pi^+$ invariant mass to be within 50 MeV/c^2 of the K^{*+} nominal mass. For continuum background suppression, in addition to the $|\cos\theta_{\rm thr}| < 0.8$ condition (which retains 80% of the signal and rejects 90% of the continuum background), we require that the K^{*+} helicity angle satisfy $|\cos\theta_{\rm hel}| > 0.4$. The K^{*+} helicity angle is defined as the angle between the axis of the K^{*+} decay products, and the momentum of the B meson, in the K^{*+} rest frame. The K^{*+} helicity requirement retains 81% of the signal and rejects 40% of the continuum background that satisfies the $|\cos\theta_{\rm thr}| < 0.8$ condition. We also apply a requirement on the Fisher discriminant that retains 95% of the signal and rejects 30% of the remaining continuum background. Figures 1(e) and 1(f) show the ΔE and $M_{\rm bc}$ distributions for $B^+ \to DK^{*+}$ candidates. The selection efficiency is 4.1%. The number of events in the signal box is 78. The parametrization of background and signal shapes is the same as that used in the $B^+ \to DK^+$ case, but without the contribution of K/π misidentification background. The number of events in the signal peak obtained from the fit is 54 $\pm$ 8; the event purity in the signal box is 65%.

III. DETERMINATION OF THE $\bar{D}^0 \to K^0_S\pi^+\pi^-$ DECAY AMPLITUDE

The amplitude f for the $\bar{D}^0 \to K^0_S\pi^+\pi^-$ decay is described by a coherent sum of two-body decay amplitudes and one nonresonant decay amplitude,

$$f(m_+^2, m_-^2) = \sum_{j=1}^{N} a_j e^{i\xi_j} \mathcal{A}_j(m_+^2, m_-^2) + a_{\rm NR} e^{i\xi_{\rm NR}}, \quad (3)$$

where N is the total number of resonances, $\mathcal{A}_j(m_+^2, m_-^2)$ is the matrix element, a_j and ξ_j are the amplitude and phase of the matrix element, respectively, of the jth resonance, and $a_{\rm NR}$ and $\xi_{\rm NR}$ are the amplitude and phase of the nonresonant component. The total phase and amplitude are arbitrary. To be consistent with other analyses [12,19] we have chosen the $\bar{D}^0 \to K^0_S\rho$ mode to have unit amplitude and zero relative phase. The description of the matrix elements follows Ref. [20].

We use a set of 18 two-body amplitudes. These include five Cabibbo-allowed amplitudes: $K^*(892)^+\pi^-$, $K^*(1410)^+\pi^-$, $K_0^*(1430)^+\pi^-$, $K_2^*(1430)^+\pi^-$ and $K^*(1680)^+\pi^-$; their doubly Cabibbo-suppressed partners; and eight amplitudes with K^0_S and a $\pi\pi$ resonance: $K^0_S\rho$, $K^0_S\omega$, $K^0_Sf_0(980)$, $K^0_Sf_2(1270)$, $K^0_Sf_0(1370)$, $K^0_S\rho(1450)$, $K^0_S\sigma_1$ and $K^0_S\sigma_2$. The differences from our previous pub-

lication [10] are (i) the addition of $K^0_S\rho(1450)$, $K^*(1410)^+\pi^-$ and the corresponding doubly Cabibbo-suppressed mode, (ii) the use of the Gounaris-Sakurai [21] amplitude description for the $K^0_S\rho$ and $K^0_S\rho(1450)$ contributions, and (iii) the mass and width for the $f_0(1370)$ state are now taken from Ref. [22] ($M = 1434\ \mathrm{MeV}/c^2$, $\Gamma = 173\ \mathrm{MeV}/c^2$).

We use an unbinned maximum likelihood technique to fit the Dalitz plot distribution to the model described by Eq. (3). We minimize the negative logarithm of the likelihood function in the form

$$-2\log L = -2\Big[\sum_{i=1}^{n}\log p(m^2_{+,i}, m^2_{-,i}) - \log\int_D p(m^2_+, m^2_-)dm^2_+\,dm^2_-\Big], \quad (4)$$

where i runs over all selected event candidates, and $m^2_{+,i}$, $m^2_{-,i}$ are measured Dalitz plot variables. The integral in the second term accounts for the overall normalization of the probability density.

The Dalitz plot density is represented by

$$p(m^2_+, m^2_-) = \varepsilon(m^2_+, m^2_-)|f(m^2_+, m^2_-)|^2 + B(m^2_+, m^2_-), \quad (5)$$

where $f(m^2_+, m^2_-)$ is the decay amplitude described by Eq. (3), $\varepsilon(m^2_+, m^2_-)$ is the efficiency, and $B(m^2_+, m^2_-)$ is the background density. To take into account the finite momentum resolution of the detector, the Dalitz plot density described by Eq. (5) is convolved with a resolution function. The free parameters of the minimization are the amplitudes a_j and phases ξ_j of the resonances (except for the $K^0_S\rho$ component, for which the parameters are fixed), the amplitude a_{NR} and phase ξ_{NR} of the nonresonant component and the masses and widths of the σ_1 and σ_2 scalars.

The procedures for determining the background density, the efficiency, and the resolution of the squared invariant mass, are the same as in the previous analyses [10,11]. The background density for $\bar{D}^0 \to K^0_S\pi^+\pi^-$ events is extracted from ΔM sidebands: $\Delta M < 142\ \mathrm{MeV}/c^2$ and $148\ \mathrm{MeV}/c^2 < \Delta M < 150\ \mathrm{MeV}/c^2$. The shape of the efficiency over the Dalitz plot, as well as the invariant mass resolution, is extracted from a MC simulation where the $\bar{D}^0$

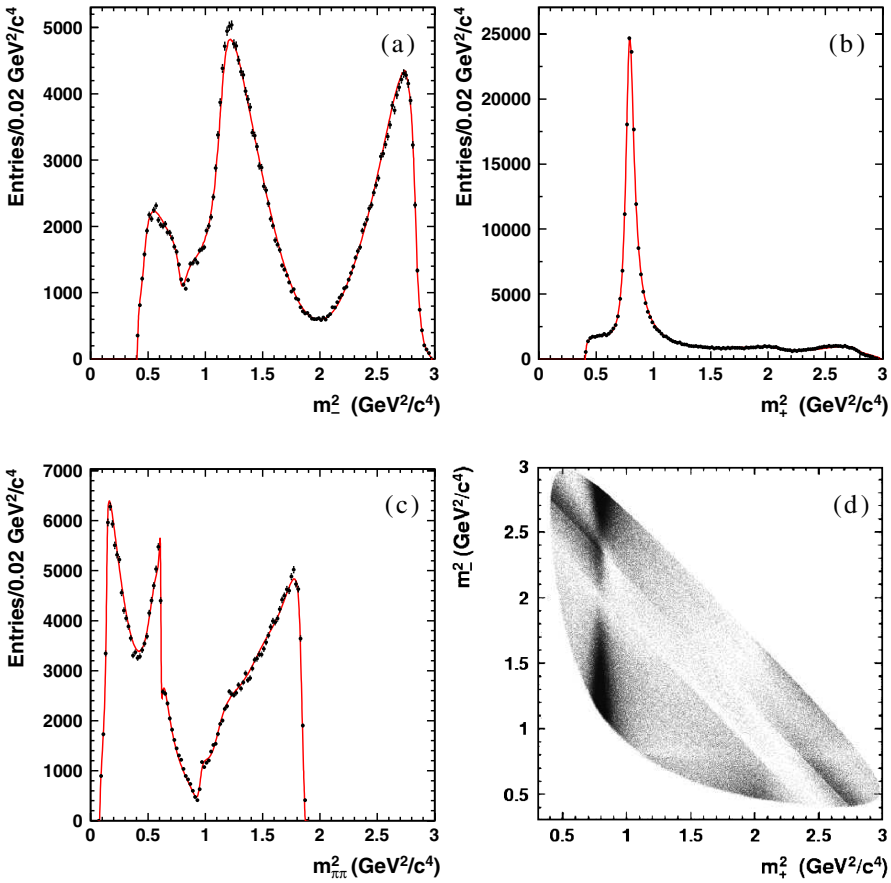

FIG. 2 (color online). (a) m^2_-, (b) m^2_+, (c) $m^2_{\pi\pi}$ and (d) Dalitz plot distribution for $D^{*-} \to \bar{D}^0\pi^-_s$, $\bar{D}^0 \to K^0_S\pi^+\pi^-$ decays from the $e^+e^- \to c\bar{c}$ continuum process. The points with error bars show the data; the smooth curve is the fit result.

decays uniformly over the allowed phase space. The resolution in $m^2_{\pi\pi}$ is extracted from the MC simulation; we consider only the resolution in $m^2_{\pi\pi}$, as the only structure in our model with a width comparable to the invariant mass resolution is due to $\omega \to \pi^+\pi^-$.

The $\bar{D}^0 \to K^0_S\pi^+\pi^-$ Dalitz plot distribution, as well as its projections with the fit results superimposed, are shown in Fig. 2. The fit results are given in Table I. The fit fractions quoted in Table I for specific modes are defined as the integral of the absolute value squared of the individual mode divided by the integral of the absolute value squared of the total amplitude. Because of the interference effects these fit fractions do not sum to unity.

The parameters obtained for the σ_1 resonance ($M_{\sigma_1} = 519 \pm 6$ MeV/c^2, $\Gamma_{\sigma_1} = 454 \pm 12$ MeV/c^2) are similar to those observed by other experiments [19,23]. The second scalar term σ_2 is introduced to account for structure observed at $m^2_{\pi\pi} \sim 1.1$ GeV$^2/c^4$: the fit finds a small but significant contribution with $M_{\sigma_2} = 1050 \pm 8$ MeV/c^2, $\Gamma_{\sigma_2} = 101 \pm 7$ MeV/c^2 (the errors are statistical only). The large peak in the m^2_+ distribution corresponds to the dominant $\bar{D}^0 \to K^*(892)^+\pi^-$ mode. The minimum in the m^2_- distribution at 0.8 GeV$^2/c^4$ is due to destructive interference with the doubly Cabibbo-suppressed $\bar{D}^0 \to K^*(892)^-\pi^+$ amplitude. In the $m^2_{\pi\pi}$ distribution, the $\bar{D}^0 \to K^0_S\rho$ contribution is visible around 0.5 GeV$^2/c^4$ with a steep edge on the upper side due to interference with $\bar{D}^0 \to K^0_S\omega$. The minimum around 0.9 GeV$^2/c^4$ is due to the decay $\bar{D}^0 \to K^0_S f_0(980)$ interfering destructively with other modes.

TABLE I. Fit results for $\bar{D}^0 \to K^0_S\pi^+\pi^-$ decay. Errors are statistical only.

Intermediate state	Amplitude	Phase (°)	Fit fraction
$K^0_S\sigma_1$	1.43 ± 0.07	212 ± 3	9.8%
$K^0_S\rho^0$	1.0 (fixed)	0 (fixed)	21.6%
$K^0_S\omega$	0.0314 ± 0.0008	110.8 ± 1.6	0.4%
$K^0_S f_0(980)$	0.365 ± 0.006	201.9 ± 1.9	4.9%
$K^0_S\sigma_2$	0.23 ± 0.02	237 ± 11	0.6%
$K^0_S f_2(1270)$	1.32 ± 0.04	348 ± 2	1.5%
$K^0_S f_0(1370)$	1.44 ± 0.10	82 ± 6	1.1%
$K^0_S\rho^0(1450)$	0.66 ± 0.07	9 ± 8	0.4%
$K^*(892)^+\pi^-$	1.644 ± 0.010	132.1 ± 0.5	61.2%
$K^*(892)^-\pi^+$	0.144 ± 0.004	320.3 ± 1.5	0.55%
$K^*(1410)^+\pi^-$	0.61 ± 0.06	113 ± 4	0.05%
$K^*(1410)^-\pi^+$	0.45 ± 0.04	254 ± 5	0.14%
$K^*_0(1430)^+\pi^-$	2.15 ± 0.04	353.6 ± 1.2	7.4%
$K^*_0(1430)^-\pi^+$	0.47 ± 0.04	88 ± 4	0.43%
$K^*_2(1430)^+\pi^-$	0.88 ± 0.03	318.7 ± 1.9	2.2%
$K^*_2(1430)^-\pi^+$	0.25 ± 0.02	265 ± 6	0.09%
$K^*(1680)^+\pi^-$	1.39 ± 0.27	103 ± 12	0.36%
$K^*(1680)^-\pi^+$	1.2 ± 0.2	118 ± 11	0.11%
nonresonant	3.0 ± 0.3	164 ± 5	9.7%

We perform a χ^2 test to check the quality of the fit, dividing the Dalitz plot into square regions 0.05×0.05 GeV$^2/c^4$. The test finds a reduced chi-square $\chi^2/ndf = 2.72$ for 1081 degrees of freedom (ndf), which is large. Examining Fig. 2, we find that the main features of the Dalitz plot are well reproduced, with some significant but numerically small discrepancies at peaks and dips of the distribution. In our final results we include a conservative contribution to the systematic error due to uncertainties in the $\bar{D}^0$ decay model, discussed in Sec. IV G.

IV. DALITZ PLOT ANALYSIS OF $B^+ \to D^{(*)}K^{(*)+}$ DECAYS

In our previous analyses, the two Dalitz distributions corresponding to the decays of B^+ and B^- were fitted simultaneously to give the parameters r, ϕ_3 and δ. Confidence intervals were then calculated using a frequentist technique, relying on toy MC simulation. In this approach, there was a bias in the fitted value of the (positive definite) parameter r, and the errors on ϕ_3 and δ were also r-dependent.

In the present analysis, we use a method similar to that of *BABAR* [12]: fitting the Dalitz distributions of the B^+ and B^- samples separately, using Cartesian parameters $x_\pm = r_\pm \cos(\pm\phi_3 + \delta)$ and $y_\pm = r_\pm \sin(\pm\phi_3 + \delta)$, where the indices "+" and "−" correspond to B^+ and B^- decays, respectively. Note that in this approach the amplitude ratios (r_+ and r_-) are not constrained to be equal for the B^+ and B^- samples. Confidence intervals in r, ϕ_3 and δ are then obtained from the $(x_\pm, y_\pm)$ using a frequentist technique. The advantage of this approach is low bias and simple distributions of the fitted parameters, at the price of fitting in a space with higher dimensionality (x_+, y_+, x_-, y_-) than that of the physical parameters (r, ϕ_3, δ); see Sec. IV E.

The fit to a single Dalitz distribution with free parameters x and y is performed by minimizing the negative unbinned likelihood function

$$-2\log L = -2\Bigg[\sum_{i=1}^{n} \log p(m^2_{+,i}, m^2_{-,i}, \Delta E_i, M_{\mathrm{bc},i}) - \log \int_D p(m^2_+, m^2_-, \Delta E, M_{\mathrm{bc}}) \times dm^2_+\, dm^2_-\, d\Delta E\, dM_{\mathrm{bc}}\Bigg], \quad (6)$$

with the Dalitz distribution density p represented as

$$p(m^2_+, m^2_-, \Delta E, M_{\mathrm{bc}}) = \varepsilon(m^2_+, m^2_-)|f(m^2_+, m^2_-) + (x+iy)f(m^2_-, m^2_+)|^2 F_{\mathrm{sig}}(\Delta E, M_{\mathrm{bc}}) + F_{\mathrm{bck}}(m^2_+, m^2_-, \Delta E, M_{\mathrm{bc}}), \quad (7)$$

where F_{sig} is the signal distribution as a function of ΔE and M_{bc} (represented by the product of two Gaussian shapes), F_{bck} is the distribution of the background, and $\varepsilon(m^2_+, m^2_-)$

is the efficiency distribution over the phase space. As in the study of the sample from continuum $D^{*-} \to \bar{D}^0 \pi_s^-$ decays, the finite momentum resolution is taken into account by convolving the function (7) with a Gaussian resolution function. The efficiency and the momentum resolution were extracted from the signal MC sample, where the neutral D meson decays according to phase space. The determination of the background contribution and efficiency profile is described below.

A. Backgrounds

To take backgrounds into account in the analysis, their Dalitz plot distributions, $\Delta E - M_{\rm bc}$ distributions (which in general may depend on Dalitz plot region) and relative fractions have to be known. The backgrounds are divided into three categories:

(i) Continuum background
(ii) $B^+ \to D^{(*)}\pi^+$ background (with π/K misidentification). This background is relevant only for the $B^+ \to DK^+$ and $B^+ \to D^*K^+$ modes.
(iii) Other $B\bar{B}$ backgrounds.

Continuum background (from the process $e^+e^- \to q\bar{q}$, where $q = u,\ d,\ s,\ c$) gives the largest contribution. It includes both pure combinatorial background, and continuum D^0 mesons combined with a random kaon. This type of background is studied in data with $\cos\theta_{\rm thr}$ and Fisher discriminant requirements applied to select continuum events. To check that the Dalitz plot shape of the continuum background selected using these requirements corresponds to that of the signal region, we use a MC sample that includes $e^+e^- \to q\bar{q}$ $(q = u, d, s, c)$ decays. The Dalitz plot distribution of the continuum background is parametrized by a third-order polynomial in the variables m_+^2 and m_-^2 (which represents the combinatorial component) and a sum of D^0 and $\bar{D}^0$ shapes for real neutral D mesons combined with random kaons.

The $B^+ \to D^{(*)}\pi^+$ process with a pion misidentified as a kaon is suppressed by the requirements on the K/π identification variable $\mathcal{R}_{\rm PID}$ and the CM energy difference. The fraction of this background is obtained by fitting the $\Delta E - M_{\rm bc}$ distribution; the corresponding Dalitz plot distribution is that of a D^0 without the opposite flavor admixture.

Other $B\bar{B}$ backgrounds, of which the dominant fraction comes from the decay of $D^{(*)0}$ from one B meson, with some particles taken from the other B decay, are investigated with $e^+e^- \to \Upsilon(4S) \to B\bar{B}$ MC events. The Dalitz plot distribution of the $B\bar{B}$ background is parametrized by a second-order polynomial (for the $B^+ \to DK^+$ and $B^+ \to DK^{*+}$ modes) or by a linear function (for the $B^+ \to D^*K^+$ mode) of m_+^2 and m_-^2, plus a "correct-flavor" D^0 shape ($\bar{D}^0$ for B^+ data and D^0 for B^- data).

B. Efficiency

Knowledge of the absolute value of the reconstruction efficiency is not essential for our analysis. However, the relative variations of the efficiency over the D^0 decay phase space can affect the fit result. The shapes of the efficiency across the phase space are studied for each mode using signal MC samples with a constant $\bar{D}^0 \to K_S^0\pi^+\pi^-$ decay amplitude. The efficiency profiles are fitted with third-order polynomial functions of m_+^2 and m_-^2 symmetric under exchange of π^+ and π^-. The efficiency is nearly flat over the phase space, falling by 10%–20% at its edges (relative to the efficiency at the center).

C. Control sample fits

To test the consistency of the fitting procedure, the same procedure was applied to the $B^+ \to \tilde{D}_+^{(*)}\pi^+$ and $B \to D^{*-}\pi^+$ control samples as to the $B^+ \to \tilde{D}_+^{(*)}K^{(*)+}$ signal. For decays to which only one D flavor can contribute, the fit should return values of the amplitude ratio r consistent with zero. In the case of $B^+ \to \tilde{D}_+^{(*)}\pi^+$ a small amplitude ratio $r \sim 0.01$ is expected (due to the small ratio of the weak coefficients $|V_{ub}V_{cd}^*|/|V_{cb}V_{ud}^*| \sim 0.02$ and the additional color suppression factor as in the case of $B^+ \to \tilde{D}_+K^+$). Deviations from these values can appear if the Dalitz plot distribution is not well described by the fit model.

For the control sample fits, we treat B^+ and B^- data separately, to check for the absence of CP violation. The free parameters of the Dalitz plot fit are $x_\pm$ and $y_\pm$.

The fit results for the three test samples are presented in Table II; contour plots showing integer multiples of the standard deviation in the $x_\pm$ and $y_\pm$ variables for the three test samples are shown in Fig. 3. The results are consistent with $r \sim 0.01$ for the $B^+ \to D\pi^+$ and $B^+ \to D^*\pi^+$ modes and with zero for the $B \to D^{*-}\pi^+$ mode.

D. Signal fit results

The Dalitz distributions of $B^+ \to \tilde{D}_+K^+$, $B^+ \to \tilde{D}_+^*K^+$, and $B^+ \to \tilde{D}_+K^{*+}$ modes for the events in the signal region used in the fits are shown in Fig. 4. The results of the separate B^+ and B^- data fits are shown in Fig. 5. The

TABLE II. Results of fits to test samples in parameters (x, y). Errors are statistical only.

Mode	x_-	y_-	x_+	y_+
$B^+ \to D\pi^+$	-0.030 ± 0.015	-0.014 ± 0.016	-0.003 ± 0.014	-0.021 ± 0.018
$B^+ \to D^*\pi^+$	-0.007 ± 0.035	-0.078 ± 0.039	0.004 ± 0.032	0.022 ± 0.039
$B \to D^{*-}\pi^+$	0.016 ± 0.030	0.014 ± 0.030	0.026 ± 0.026	0.009 ± 0.036

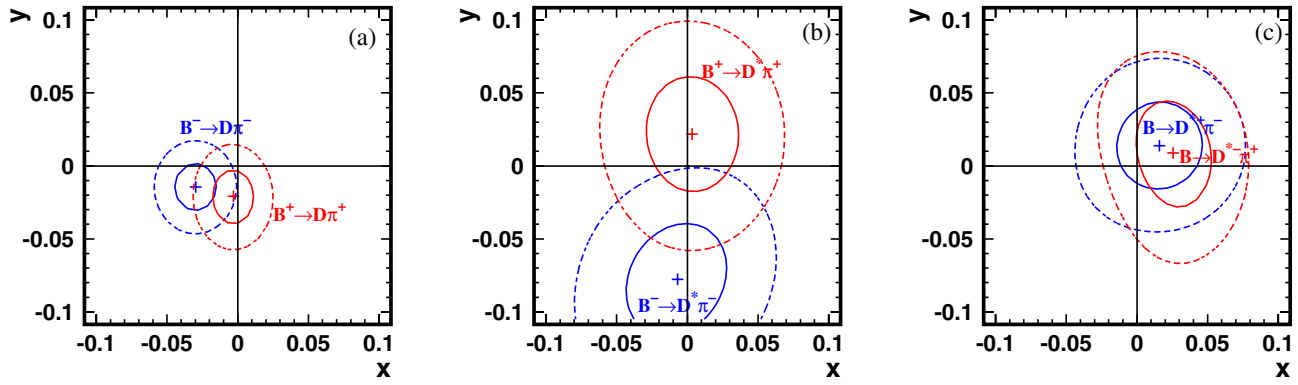

FIG. 3 (color online). Results of test sample fits with free parameters $x = r\cos\theta$ and $y = r\sin\theta$ for (a) $B^+ \to D\pi^+$, (b) $B^+ \to D^*\pi^+$ and (c) $B \to D^{*-}\pi^+$ samples, separately for B^- and B^+ data. Contours indicate integer multiples of the standard deviation.

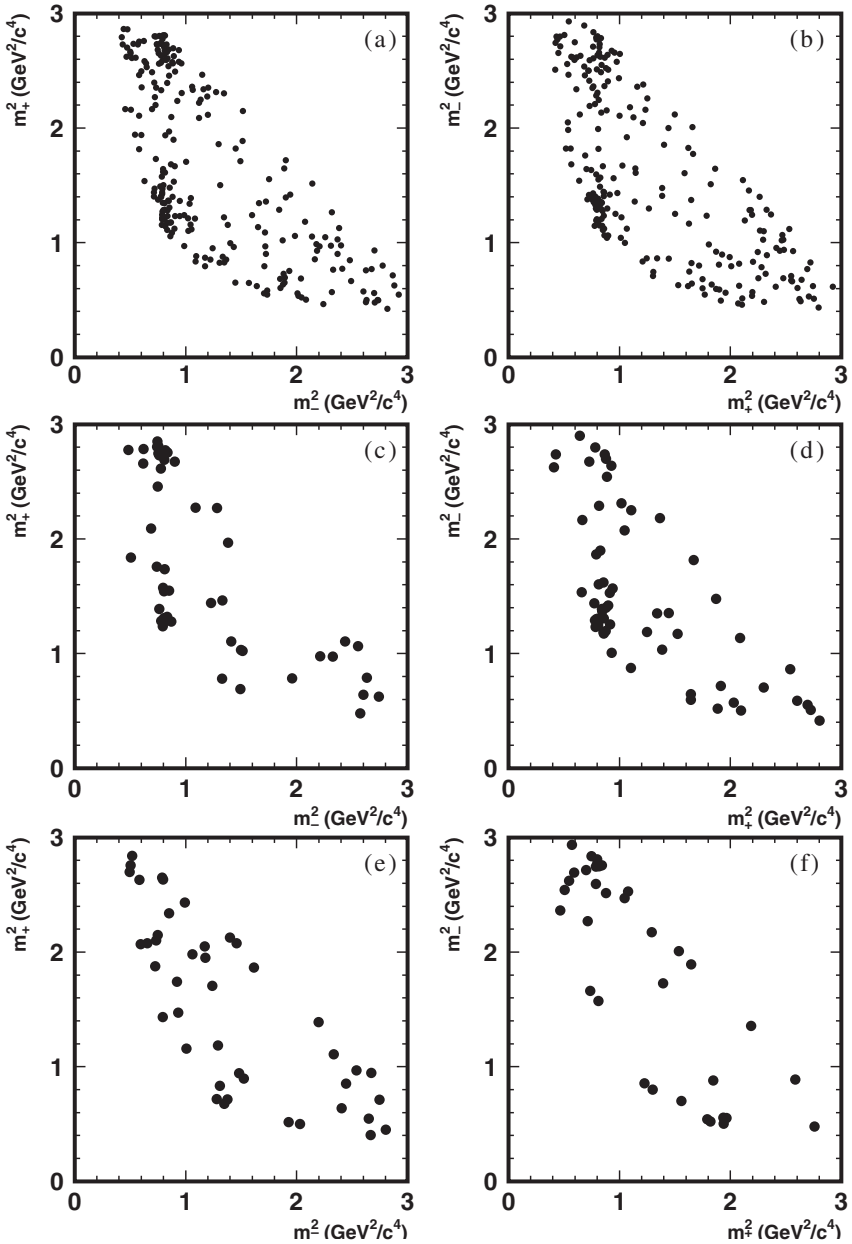

FIG. 4. Dalitz plots for the neutral D meson from (left) B^- and (right) B^+ decays, for the (a,b) $B^+ \to DK^+$, (c,d) $B^+ \to D^*K^+$, and (e,f) $B^+ \to DK^{*+}$ modes. Note that the axes are flipped in the case of B^- with respect to B^+.

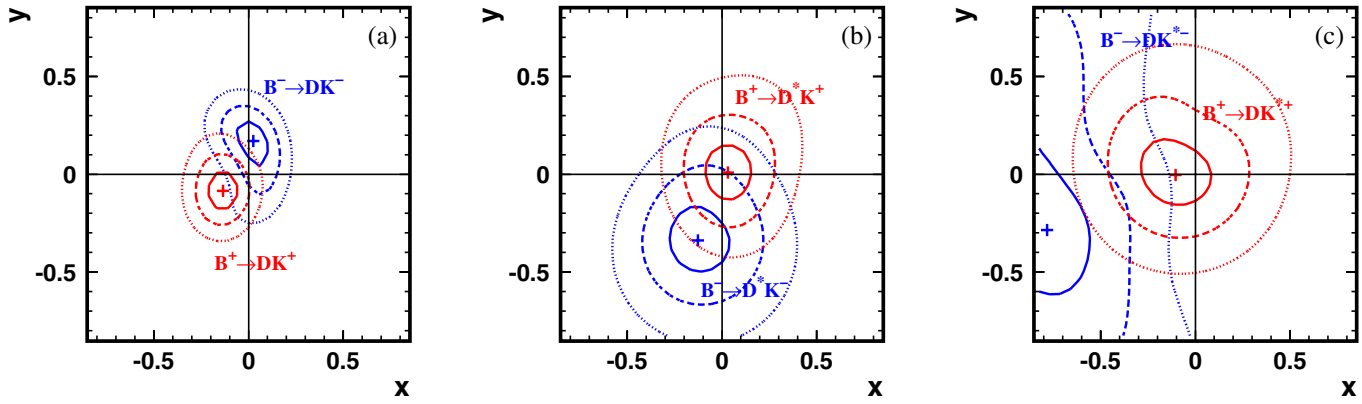

FIG. 5 (color online). Results of signal fits with free parameters $x = r\cos\theta$ and $y = r\sin\theta$ for (a) $B^+ \to DK^+$, (b) $B^+ \to D^*K^+$ and (c) $B^+ \to DK^{*+}$ samples, separately for B^- and B^+ data. Contours indicate integer multiples of the standard deviation.

plots show the constraints on the parameters x and y for the $B^+ \to \tilde{D}_+ K^+$, $B^+ \to \tilde{D}^*_+ K^+$ and $B^+ \to \tilde{D}_+ K^{*+}$ samples. The values of the fit parameters $x_\pm$ and $y_\pm$ are listed in Table III.

The fit to the $B^+ \to DK^+$ sample yields r_+ and r_- values close to each other ($r_+ = 0.172$ and $r_- = 0.160$) with significantly different values of the total phase $\theta_+ = \delta + \phi_3$ and $\theta_- = \delta - \phi_3$, which is an indication of CP violation. For the $B^+ \to D^*K^+$ and $B^+ \to DK^{*+}$ samples, the values of r_+ and r_- differ (with large errors); in both cases, r_+ is within a standard deviation of zero, so the corresponding phase θ_+ is poorly determined and the significance of CP violation is low.

E. Evaluation of statistical error

We use a frequentist technique to evaluate the statistical significance of the measurements. This method requires knowledge of the probability density function (PDF) of the reconstructed parameters x and y as a function of the true parameters $\bar{x}$ and $\bar{y}$. To obtain this PDF, we employ a ''toy'' MC technique that uses a simplified MC simulation of the experiment which incorporates the same efficiencies, resolution and backgrounds as used in the fit to the experimental data.

For each mode, 4000 toy MC experiments are made with generated $(\bar{x}, \bar{y})$ equal to the experimental fit results. The PDFs obtained are approximately Gaussian, but we observe the width of the distribution to vary with $\bar{x}$ and $\bar{y}$. There is also an offset in the parameters x, y introduced by the fit procedure. The correlations between x and y are negligible. For the $B^+ \to DK^+$ and $B^+ \to D^*K^+$ modes, the deviations from the Gaussian shape are small, and taking into account the tails of the distributions has only a minor effect on the fit result. However, the result of the measurement in the $B^- \to DK^{*-}$ mode has a relatively large value of r ($r_- = 0.83 \pm 0.28$). For such a large value, the toy MC study shows the existence of significant tails in the observed x and y distributions. To parametrize the shapes of the x and y distributions for the $B^+ \to DK^{*+}$ sample we perform additional toy MC simulation for different generated $\bar{x}$ and $\bar{y}$, and fit the distributions with the sum of two Gaussians (''narrow'' and ''wide''). To obtain the PDF shape for any given set of $(\bar{x}, \bar{y})$, linear interpolation in $\bar{x}$ and $\bar{y}$ (for the bias of the wide Gaussian relative to the narrow one) and in $\bar{x}^2$ and $\bar{y}^2$ (for the width and fraction of the wide Gaussian) are used.

To obtain the $(\bar{x}, \bar{y})$ dependence of σ_x and σ_y and the offset in x and y, we generate toy MC experiments at different points in the $(\bar{x}, \bar{y})$ plane, corresponding to 4 values of θ for $r = 0.15$ and 8 values of θ for $r = 0.3$ and $r = 0.6$. For the $B^+ \to DK^{*+}$ mode, an additional set of 8 points with $r = 0.9$ is added. 200 toy MC experiments are generated at each point. The standard deviation and offset are then parametrized with polynomial functions in $\bar{x}$ and $\bar{y}$.

The offset in x and y is large enough to affect the result of the measurement (up to 0.02 for the $B^\pm \to DK^\pm$ mode); it is larger in the $B^+ \to D^*K^+$ and $B^+ \to DK^{*+}$ modes, where the data samples are smaller. To test the effect of sample size, toy MC experiments were generated with event samples 10 times larger than those of the $B^\pm \to DK^\pm$ data: the offset for this sample is less than 5×10^{-3}. This is consistent with the maximum likelihood fit

TABLE III. Results of the signal fits in parameters (x, y). Errors are statistical only.

Mode	x_-	y_-	x_+	y_+
$B^+ \to DK^+$	$0.025^{+0.072}_{-0.080}$	$0.170^{+0.093}_{-0.117}$	$-0.135^{+0.069}_{-0.070}$	$-0.085^{+0.090}_{-0.086}$
$B^+ \to D^*K^+$	$-0.128^{+0.167}_{-0.146}$	$-0.339^{+0.172}_{-0.158}$	$0.032^{+0.120}_{-0.116}$	$0.008^{+0.137}_{-0.136}$
$B^+ \to DK^{*+}$	$-0.784^{+0.249}_{-0.295}$	$-0.281^{+0.440}_{-0.335}$	$-0.105^{+0.177}_{-0.167}$	$-0.004^{+0.164}_{-0.156}$

being unbiased in the limit of large sample sizes. For each mode, the offset is included in the PDF for the reconstructed parameters, so the confidence intervals (and central values) for ϕ_3, r, δ are unbiased.

Different implementations of the frequentist technique can be used to obtain the values of the physical parameters. The two most widely used are central (so-called Neyman) intervals, and the unified approach of Feldman and Cousins [24]. The latter takes unphysical regions of the parameter space into account. In this analysis, fitting with four parameters $(x_\pm, y_\pm)$ in a problem defined by three parameters (r, ϕ_3, δ) creates an unphysical region: all $(x_\pm, y_\pm)$ values where $r_+ \neq r_-$. For two of the three samples ($B^+ \to D^* K^+$ and $B^+ \to D K^{*+}$) the values of r_+ and r_- differ significantly, i.e. the result for these modes is well into the unphysical region. Central intervals would overestimate the significance of the measurement in this case. Therefore, to obtain the values of the physical parameters r, ϕ_3 and δ (we will refer to this set of parameters as a vector $\boldsymbol{\mu}$) given the measurement result x_+, y_+, x_- and y_- (or vector z) we use the Feldman-Cousins approach.

The confidence level α is calculated as

$$\alpha(\boldsymbol{\mu}) = \int_{\mathcal{D}(\boldsymbol{\mu})} p(z|\boldsymbol{\mu}) dz, \tag{8}$$

where the integration domain $\mathcal{D}$ is given by likelihood ratio ordering:

$$\frac{p(z|\boldsymbol{\mu})}{p(z|\boldsymbol{\mu}_{\rm best}(z))} > \frac{p(z_0|\boldsymbol{\mu})}{p(z_0|\boldsymbol{\mu}_{\rm best}(z_0))}. \tag{9}$$

Here, $p(z|\boldsymbol{\mu})$ is the normalized probability density to obtain the measurement result z for a given set of true parameters $\boldsymbol{\mu}$. This PDF is obtained by toy MC simulation. $\boldsymbol{\mu}_{\rm best}(z)$ stands for the best true parameters for a given measurement z, i.e. $\boldsymbol{\mu}$ such that $p(z|\boldsymbol{\mu})$ is maximized for the given z. z_0 is the result of the fit to experimental data.

Figure 6 shows the projections of the three-dimensional confidence regions onto (r, ϕ_3) and (ϕ_3, δ) planes. We show the 20%, 74% and 97% confidence level regions, which correspond to 1, 2, and 3 standard deviations for a three-dimensional Gaussian distribution. The central values for the parameters r, ϕ_3 and δ with their 1 and 2 standard deviation intervals are presented in Table IV. The confidence intervals in Table IV are calculated from projections of the three-dimensional confidence regions onto each of the parameters. Toy MC studies of the $B^\pm \to D K^\pm$ mode show that these intervals include the true value of ϕ_3 slightly more often than the confidence levels imply (overcoverage), and are therefore conservative.

F. Estimation of systematic errors

Experimental systematic errors come from uncertainty in the knowledge of the functions used in the signal Dalitz plot fit. These include the Dalitz plot profiles of the backgrounds and the detection efficiency, the momentum resolution description, and, since the background fraction varies depending on the ΔE and $M_{\rm bc}$ parameters, the parametrizations of the $\Delta E - M_{\rm bc}$ shape of the signal and background.

The systematic errors related to the Dalitz plot shape of the background are studied by using different background descriptions in the signal fit. In the baseline background shape, the continuum component is determined from the continuum-enriched data sample, and the $B\bar{B}$ background is based on a MC sample. In addition, we perform fits with the background shape represented by only the continuum background parametrization, and the background shape extracted from the $M_{\rm bc}$ sideband ($5.2\ {\rm GeV}/c^2 < M_{\rm bc} < 5.26\ {\rm GeV}/c^2$). The maximum deviation of the parameters x, y from those obtained with the ''standard'' background parametrization was taken as a measure of the systematic error.

The distribution of the relative detection efficiency over the Dalitz plot is obtained from the MC simulation. To estimate the effect of imperfect simulation of the detector response, we also attempt to obtain the efficiency shape from the experimental data. We expect that the detection efficiency depends primarily on the momentum of the D meson. We also assume that for high momentum D mesons, the efficiency does not vary significantly over phase space and is well determined in the simulation. Therefore, to obtain the relative efficiency distribution for, e.g. the $B^+ \to D K^+$ sample, we use the continuum $D^{*-} \to \bar{D}^0 \pi_s^-$ sample with $\bar{D}^0 \to K_S^0 \pi^+ \pi^-$ (the one used for the determination of the $\bar{D}^0 \to K_S^0 \pi^+ \pi^-$ amplitude) and compare Dalitz plots for high momentum $\bar{D}^0$ ($p_D > 3.5\ {\rm GeV}/c$ in the CM frame) and $\bar{D}^0$ in the momentum range corresponding to the $B^+ \to D K^+$ decay ($2.1\ {\rm GeV}/c < p_D < 2.4\ {\rm GeV}/c$ in the CM frame). If the background is subtracted, the ratio of the event densities for the decays of $\bar{D}^0$ in different momentum ranges should equal the ratio of detection efficiencies. Once we assume that the efficiency for high momentum $\bar{D}^0$ is known, the efficiency distribution of $\bar{D}^0$ from $B^+ \to D K^+$ decay can be calculated. The difference of the parameters x, y between fits using MC-based and data-based efficiency shapes is taken as the corresponding systematic error.

The uncertainty due to momentum resolution is estimated by performing a $\bar{D}^0$ model fit with a subsequent fit to B decay data without taking the momentum resolution into account. The bias of the (x, y) parameters is negligible, therefore, this systematic uncertainty is neglected.

The uncertainty of the $\Delta E - M_{\rm bc}$ distribution parametrization (which, in particular, leads to uncertainty in the signal-to-background ratio) is taken into account by performing fits using $\Delta E - M_{\rm bc}$ shapes with each of the parameters varied by 1 standard deviation.

The $\Delta E - M_{\rm bc}$ shape and the total background fraction are extracted from the signal $\Delta E - M_{\rm bc}$ fit. Both continuum and $B\bar{B}$ backgrounds are parametrized by a common

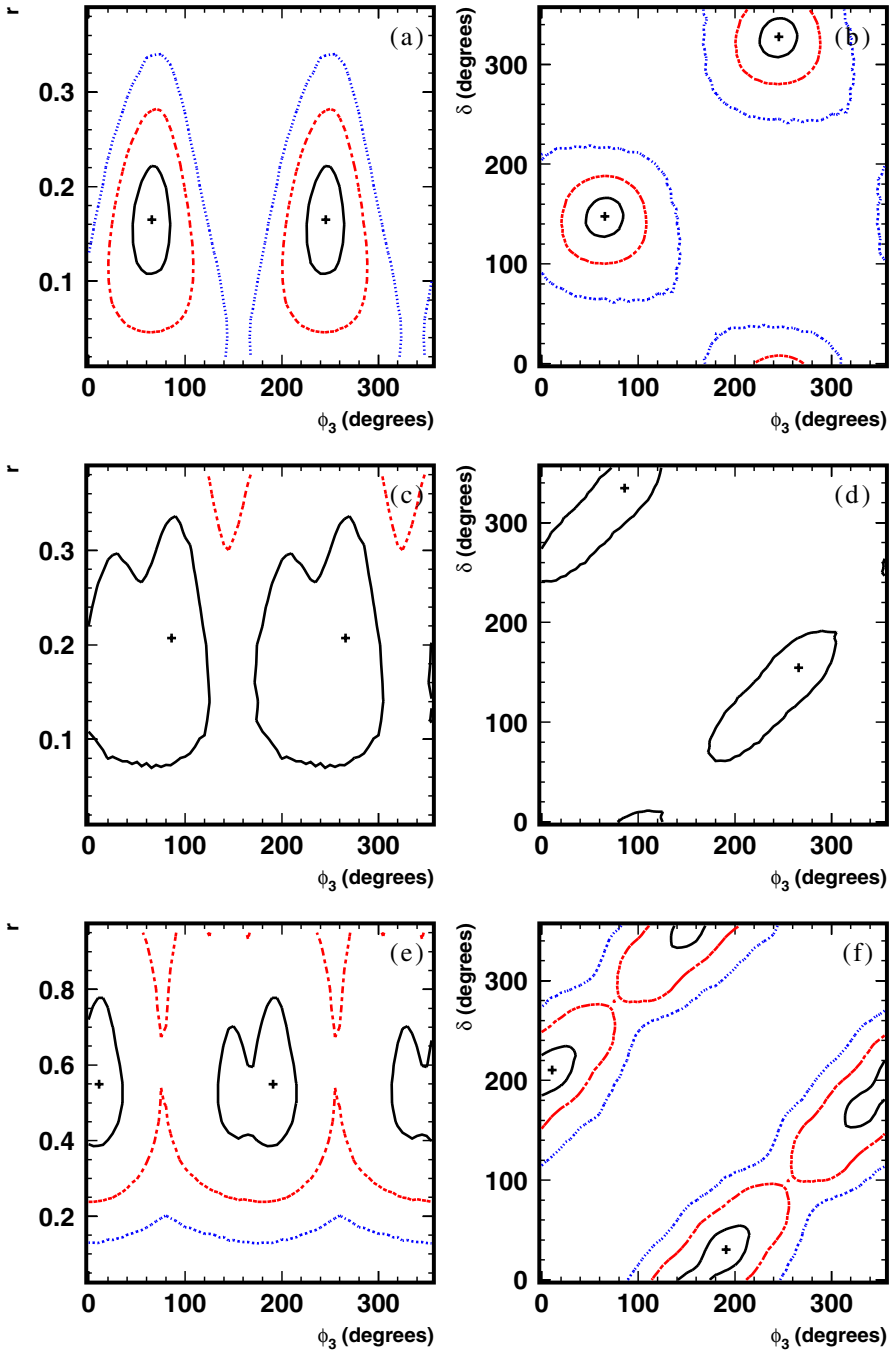

FIG. 6 (color online). Projections of confidence regions for the (a,b) $B^+ \to DK^+$, (c,d) $B^+ \to D^*K^+$, and (e,f) $B^+ \to DK^{*+}$ modes onto the (r, ϕ_3) and (ϕ_3, δ) planes. Contours indicate integer multiples of the standard deviation.

TABLE IV. *CP* fit results. The error intervals are statistical only.

Parameter	$B^+ \to DK^+$ mode		$B^+ \to D^*K^+$ mode		$B^+ \to DK^{*+}$ mode	
	1σ interval	2σ interval	1σ interval	2σ interval	1σ interval	2σ interval
ϕ_3	$65.5^\circ\ ^{+19.1^\circ}_{-19.9^\circ}$	$20.8^\circ < \phi_3 < 108.4^\circ$	$86.1^\circ\ ^{+37.1^\circ}_{-93.1^\circ}$	-	$10.8^\circ\ ^{+22.7^\circ}_{-57.1^\circ}$	-
r	$0.165^{+0.056}_{-0.059}$	$0.048 < r < 0.281$	$0.207^{+0.127}_{-0.131}$	$r < 0.510$	$0.549^{+0.231}_{-0.163}$	$0.242 < r < 1.120$
δ	$147.5^\circ\ ^{+18.7^\circ}_{-20.3^\circ}$	$100.3^\circ < \delta < 187.7^\circ$	$334.7^\circ\ ^{+36.8^\circ}_{-93.6^\circ}$	-	$210.2^\circ\ ^{+24.2^\circ}_{-57.3^\circ}$	-

TABLE V. Systematic errors in x, y variables.

Component	$B^+ \to DK^+$ mode				$B^+ \to D^*K^+$ mode				$B^+ \to DK^{*+}$ mode			
	Δx_-	Δy_-	Δx_+	Δy_+	Δx_-	Δy_-	Δx_+	Δy_+	Δx_-	Δy_-	Δx_+	Δy_+
Background shape	0.006	0.015	0.002	0.006	0.011	0.023	0.002	0.004	0.011	0.026	0.002	0.009
Efficiency shape	0.011	0.004	0.017	0.001	0.001	0.001	0.001	0.001	0.024	0.023	0.002	0.009
$\Delta E - M_{\rm bc}$ stat. uncertainty	0.002	0.005	0.002	0.004	0.005	0.009	0.002	0.003	0.006	0.013	0.003	0.003
$\Delta E - M_{\rm bc}$ difference for $q\bar{q}$ and $B\bar{B}$	0.004	0.002	0.000	0.005	0.019	0.012	0.002	0.010	0.010	0.027	0.004	0.001
Total	0.013	0.016	0.017	0.009	0.023	0.027	0.004	0.011	0.029	0.046	0.006	0.013

$\Delta E - M_{\rm bc}$ density. However, in general, continuum and $B\bar{B}$ (and even each of the subcomponents of these backgrounds) may be distributed differently, and the distribution may be correlated with the Dalitz plot distribution. To estimate the contribution of this effect, we make additional fits to data with individual $\Delta E - M_{\rm bc}$ distributions for continuum and $B\bar{B}$ background components extracted from generic MC samples. The corresponding bias is included in the background systematic error.

The results of the study of experimental systematic errors are summarized in Table V for each mode. The uncertainties in the parameters (x, y) are then used to obtain the systematic errors for r, ϕ_3 and δ in the combined measurement (see Sec. IV H). In our previous analyses [10,11] the systematic error was dominated by a term due to the bias in the fit of (ϕ_3, r, δ) to the $B^+ \to D\pi^+$ control sample (see Ref. [10] Section V. B). In the present analysis, biases in the fit of $(x_\pm, y_\pm)$ to data are small, and are taken into account when forming confidence intervals in ϕ_3, r, and δ (section IV E). Fitted values for the $B^+ \to D^{(*)}\pi^+$ control samples are consistent with expectations (Sec. IV C), with statistical precision comparable to the systematic errors listed in Table V. No additional systematic error is assigned.

G. Estimation of model uncertainty

The model used for the $\bar{D}^0 \to K^0_S\pi^+\pi^-$ decay amplitude is one of the main sources of systematic error for our analysis. The amplitude is a result of the fit to the experimental Dalitz plot, however since the density of the plot is proportional to the absolute value squared of the decay amplitude, the phase of the complex amplitude is not directly measured. The phase variations across the Dalitz plot are therefore a function of model assumptions and their uncertainties may affect the $\tilde{D}$ Dalitz plot fit.

We use a MC simulation to estimate the effects of the model uncertainties. Event samples are generated according to the Dalitz distribution described by the amplitude given by Eq. (7) with the resonance parameters extracted from our fit to continuum $\bar{D}^0 \to K^0_S\pi^+\pi^-$ data, but to fit this distribution different models for $f(m^2_+, m^2_-)$ are used. We scan the phases ϕ_3 and δ in their physical regions and take the maximum deviations of the fit parameters $[(\Delta r)_{\rm max}$, $(\Delta\phi_3)_{\rm max}$, and $(\Delta\delta)_{\rm max}]$ as model uncertainty estimates. These studies use the value $r = 0.15$, close to the one obtained in the dominant $B^+ \to DK^+$ mode.

All the fit models are based on Breit-Wigner parametrizations of resonances as in our default model, but with differences in the treatment of the broad components. By default, we use Blatt-Weisskopf form factors for the $\bar{D}^0$ meson (F_D) and intermediate resonances (F_r) and a q^2 dependence of the resonance width Γ (see [20]): to estimate the effect of the corresponding theoretical uncertainties, we use a fit model without form-factors, and with constant resonant widths Γ_i. We also use a model containing only the largest doubly-Cabibbo-suppressed term $K^*(892)^-\pi^+$, the narrow resonances, $K^0_S f_0(980)$, and $K^*_0(1430)^+\pi^-$, with the remainder of the amplitude approximated by the flat nonresonant term.

Other models used are the model with all the resonances from Table I excluding the σ_1 or σ_2 states, and the model used by CLEO [19]. The results of the study of model uncertainty are summarized in Table VI. The maximum deviation of the parameters is taken as the uncertainty due to the $\bar{D}^0 \to K^0_S\pi^+\pi^-$ decay model. Each of the models listed in Table VI has a reduced χ^2 significantly poorer than that of the default model. Therefore, our model uncertainty does not include an additional contribution due to the poor quality of the model fit, discussed in Sec. III.

The mode $B^+ \to DK^{*+}$ has an additional uncertainty due to the possible presence of a nonresonant $B^+ \to DK^0_S\pi^+$ component, which can also be treated as a model uncertainty. Since the nonresonant decay is described by the same set of diagrams as $B^+ \to DK^{*+}$, a similar CP violating effect should be present that in general has values of r and δ which differ from those for the resonant mode. Thus, for a ϕ_3 measurement without taking the $B^+ \to DK^0_S\pi^+$ mode into account, its contribution can bias the fit parameters. To estimate the corresponding systematic uncertainty, we first measure the fraction of nonresonant decays within the $B^+ \to DK^{*+}$ signal region. To increase the sample size for this study, we include additional $\bar{D}^0$ decay modes: $K^+\pi^-$, $K^0_S\pi^+\pi^-$, $K^+\pi^-\pi^0$ and $K^+\pi^-\pi^+\pi^-$. Based on the B^+ yield in the K^{*+} mass sidebands, and the observed shape of the invariant mass $M_{K^0_S\pi^+}$ of signal candidates, we find an upper limit of 6.3% on the $B^+ \to DK^0_S\pi^+$ fraction. We then perform a toy MC simulation with a 6.3% nonresonant contribution added to

TABLE VI. Estimation of the $\bar{D}^0 \to K^0_S\pi^+\pi^-$ decay model uncertainty.

Fit model	$(\Delta r)_{\max}$	$(\Delta\phi_3)_{\max}$ (°)	$(\Delta\delta)_{\max}$ (°)
$F_r = F_D = 1$	0.01	3.1	3.3
$\Gamma(q^2) =$ constant	0.02	4.7	9.0
$K^*(892)^+$, ρ, ω, $K^*(892)^-$, $f_0(980)$, $K^*_0(1430)$, nonres.	0.05	8.5	22.9
No σ_1	0.01	2.6	4.3
No σ_2	0.01	0.6	0.7
CLEO model	0.02	5.7	8.7

determine the bias of the fit parameters. The fits are performed for various values of the r and δ parameters of the nonresonant component and various values of the relative phase between $B^\pm \to DK^{*\pm}$ and $B^\pm \to DK^0_S\pi^\pm$ amplitudes. The maximum bias of the fit parameters is taken as the corresponding systematic error: $\Delta r = 0.084$, $\Delta\phi_3 = 8.3°$, $\Delta\delta = 49.3°$. The ϕ_3 bias is significantly smaller than that for the strong phase δ, since ϕ_3 is obtained from a difference of the total phases for B^+ and B^- decays, and a part of the bias cancels in this case.

H. Combined ϕ_3 measurement

The three event samples, $B^+ \to DK^+$, $B^+ \to D^*K^+$, and $B^+ \to DK^{*+}$ are combined in order to improve the sensitivity to ϕ_3. The confidence levels for the combination of three modes are obtained using the same technique as for the single mode. In this case, the vector of physical parameters is $\boldsymbol{\mu} = (\phi_3, r_{DK}, \delta_{DK}, r_{D*K}, \delta_{D*K}, r_{DK*}, \delta_{DK*})$ and there are 12 measured parameters: four parameters $(x_\pm, y_\pm)$ for each of the three modes. The probability density of the measurement result $p(z|\boldsymbol{\mu})$ is the product of the probability densities for the individual modes.

For each $\boldsymbol{\mu}$, to obtain the confidence level $\alpha(\boldsymbol{\mu})$, the integral in Eq. (8) is performed over a 12-dimensional space. This requires extensive computation that makes it impractical to scan the whole range of physical parameters to obtain multidimensional confidence regions. However, it is still possible to calculate the confidence intervals for each of the individual parameters.

To calculate the systematic errors for the combined measurement, we vary the measured parameters x and y within their systematic errors. Gaussian distributions are used for the variation, and the systematic biases are assumed to be uncorrelated. For each of the varied parameter sets, the central values of the physical parameters are calculated. The systematic error of the physical parameter is then taken to be equal to the RMS of the resulting distribution.

The error due to the uncertainty in the $\bar{D}^0 \to K^0_S\pi^+\pi^-$ amplitude is considered to be equal in all modes. The uncertainty due to the possible contribution of the nonresonant $B^+ \to DK^0_S\pi^+$ amplitude to $B^+ \to DK^{*+}$ decay is also included in the model error, by varying the parameters $(x_\pm, y_\pm)$ of the $B^+ \to DK^{*+}$ sample according to the biases Δr, $\Delta\phi_3$, and $\Delta\delta$ obtained above (Sec. IV G). We find a contribution of only 1.8° to the combined ϕ_3 measurement; this is added in quadrature, yielding a total error of 8.7°. For the r and δ parameters of the $B^+ \to DK^{*+}$ mode the $B^+ \to DK^0_S\pi^+$ contribution dominates the model error.

Confidence intervals for the combined measurement together with systematic and model errors are shown in Table VII. The confidence intervals are statistical only and are calculated from projections of the seven-dimensional confidence regions onto each of the parameters. The statistical confidence level of CP violation is 74%. It is defined as the minimum confidence level $\alpha(\boldsymbol{\mu})$ for the CP-conserving set of physical parameters $\boldsymbol{\mu}$ (i.e. the set with $\phi_3 = 0$). The 2 standard deviation interval (including model and systematic uncertainties) is calculated by adding the doubled systematic and model errors in quadrature to the 2 standard deviation statistical errors: we find $8° < \phi_3 < 111°$.

We note that the 2 standard deviation interval of ϕ_3 is more than twice as wide as the 1 standard deviation interval. The non-Gaussian errors in ϕ_3 are related to the low

TABLE VII. Results of the combination of $B^+ \to DK^+$, $B^+ \to D^*K^+$, and $B^+ \to DK^{*+}$ modes.

Parameter	1σ statistical interval	2σ statistical interval	Systematic error	Model uncertainty
ϕ_3	$53.3° \,^{+14.8°}_{-17.7°}$	$11.7° < \phi_3 < 107.7°$	2.5°	8.7°
r_{DK}	$0.159^{+0.054}_{-0.050}$	$0.048 < r_{DK} < 0.271$	0.012	0.049
δ_{DK}	$145.7° \,^{+19.0°}_{-19.7°}$	$100.6° < \delta_{DK} < 185.9°$	3.0°	22.9°
r_{D^*K}	$0.175^{+0.108}_{-0.099}$	$0 < r_{D^*K} < 0.407$	0.013	0.049
δ_{D^*K}	$302.0° \,^{+33.8°}_{-35.1°}$	-	6.1°	22.9°
r_{DK^*}	$0.564^{+0.216}_{-0.155}$	$0.231 < r_{DK^*} < 1.106$	0.041	0.084
δ_{DK^*}	$242.6° \,^{+20.2°}_{-23.2°}$	$186.0° < \delta_{DK^*} < 300.2°$	2.5°	49.3°

significance of r; this effect should be reduced with larger data samples in the future. There is also a contribution from the disagreement between the $B^+ \to DK^+$ and $B^+ \to DK^{*+}$ results, which leads to a second minimum in $\alpha(\boldsymbol{\mu})$ between the 1 and 2 standard deviation levels.

V. CONCLUSION

We report the results of a measurement of the unitarity triangle angle ϕ_3, using a method based on Dalitz plot analysis of $\bar{D}^0 \to K^0_S\pi^+\pi^-$ decay in the process $B^+ \to D^{(*)}K^{(*)+}$. The measurement of ϕ_3 using this technique was performed based on a 357 fb^{-1} data sample collected by the Belle detector. From the combination of $B^+ \to DK^+$, $B^+ \to D^*K^+$ and $B^+ \to DK^{*+}$ modes, we obtain the value $\phi_3 = 53^\circ\,^{+15^\circ}_{-18^\circ} \pm 3^\circ \pm 9^\circ$; of the two possible solutions we choose the one with $0 < \phi_3 < 180^\circ$. The first error is statistical, the second is experimental systematics and the third is model uncertainty. The 2 standard deviation interval (including model and systematic uncertainties) is $8^\circ < \phi_3 < 111^\circ$. The statistical significance of CP violation for the combined measurement is 74%. The method allows us to obtain a value of the ratio of the two interfering D decay amplitudes r, which can be used in other ϕ_3 measurements. We obtain $r = 0.159^{+0.054}_{-0.050} \pm 0.012 \pm 0.049$ for the $B^+ \to DK^+$ mode, $r = 0.175^{+0.108}_{-0.099} \pm 0.013 \pm 0.049$ for the $B^+ \to D^*K^+$ mode and $r = 0.564^{+0.216}_{-0.155} \pm 0.041 \pm 0.084$ for the $B^+ \to DK^{*+}$ mode.

ACKNOWLEDGMENTS

We thank the KEKB group for the excellent operation of the accelerator, the KEK cryogenics group for the efficient operation of the solenoid, and the KEK computer group and the National Institute of Informatics for valuable computing and Super-SINET network support. We acknowledge support from the Ministry of Education, Culture, Sports, Science, and Technology of Japan and the Japan Society for the Promotion of Science; the Australian Research Council and the Australian Department of Education, Science and Training; the National Science Foundation of China and the Knowledge Innovation Program of Chinese Academy of Sciences under Contract No. 10575109 and IHEP-U-503; the Department of Science and Technology of India; the BK21 program of the Ministry of Education of Korea, and the CHEP SRC program and Basic Research program (Grant No. R01-2005-000-10089-0) of the Korea Science and Engineering Foundation; the Polish State Committee for Scientific Research under Contract No. 2P03B 01324; the Ministry of Science and Technology of the Russian Federation; the Slovenian Research Agency; the Swiss National Science Foundation; the National Science Council and the Ministry of Education of Taiwan; and the U.S. Department of Energy.

APPENDIX: MODEL UNCERTAINTY IN (x, y) PARAMETERS

Averaging the ϕ_3 measurements between different methods and different experiments is most conveniently done using the (x, y) parameters, which are better-behaved than (r, ϕ_3, δ). This requires errors (including model uncertainty) to be expressed in terms of the (x, y) parameters, but our model uncertainty study was performed in (r, ϕ_3, δ). To calculate the errors due to the $\bar{D}^0 \to K^0_S\pi^+\pi^-$ decay model uncertainty in (x, y) we propagate the (r, ϕ_3, δ) errors under the assumption that there is no correlation between them. This approach results in substantial off-diagonal terms. The correlation matrix for the vector $z = (x_{DK^-}, y_{DK^-}, x_{DK^+}, y_{DK^+}, x_{D^*K^-}, y_{D^*K^-}, x_{D^*K^+}, y_{D^*K^+}, x_{DK^{*-}}, y_{DK^{*-}}, x_{DK^{*+}}, y_{DK^{*+}})$ is defined as

$$(\mathcal{C}_{D^0})_{ij} = \overline{\Delta z_i \Delta z_j},$$

and is equal to

$$\mathcal{C}_{D^0} = \begin{pmatrix}
459 & 10 & -104 & 332 & -56 & 21 & 6 & 62 & -12 & 68 & 64 & 30 \\
10 & 241 & -232 & -64 & -3 & 1 & 0 & 2 & 0 & 3 & 3 & 2 \\
-104 & -232 & 264 & -68 & -18 & 7 & 2 & 20 & -3 & 22 & 20 & 10 \\
332 & -64 & -68 & 436 & 55 & -22 & -4 & -57 & 9 & -66 & -59 & -30 \\
-56 & -3 & -18 & 55 & 515 & -108 & -54 & 400 & 10 & -70 & -64 & -33 \\
21 & 1 & 7 & -22 & -108 & 282 & -235 & -135 & -4 & 27 & 25 & 13 \\
6 & 0 & 2 & -4 & -54 & -235 & 242 & 26 & -1 & 7 & 5 & 2 \\
62 & 2 & 20 & -57 & 400 & -135 & 26 & 556 & -13 & 76 & 69 & 33 \\
-12 & 0 & -3 & 9 & 10 & -4 & -1 & -13 & 939 & 36 & -328 & 878 \\
68 & 3 & 22 & -66 & -70 & 27 & 7 & 76 & 36 & 732 & -556 & -99 \\
64 & 3 & 20 & -59 & -64 & 25 & 5 & 69 & -328 & -556 & 769 & -86 \\
30 & 2 & 10 & -30 & -33 & 13 & 2 & 33 & 878 & -99 & -86 & 904
\end{pmatrix} \times 10^{-5}. \tag{A1}$$

The uncertainty due to the nonresonant contribution to the $B^+ \to DK^{*+}$ mode produces an additional contribution

$$\mathcal{C}_{DK\pi} = \begin{pmatrix} 766 & -371 & 113 & 828 \\ -371 & 2984 & -2605 & -1136 \\ 113 & -2605 & 2601 & 919 \\ 828 & -1136 & 919 & 1150 \end{pmatrix} \times 10^{-5}. \quad \text{(A2)}$$

to the terms in $(x_{DK^{*-}}, y_{DK^{*-}}, x_{DK^{*+}}, y_{DK^{*+}})$.

[1] M. Kobayashi and T. Maskawa, Prog. Theor. Phys. **49**, 652 (1973); N. Cabibbo, Phys. Rev. Lett. **10**, 531 (1963).
[2] I. I. Bigi and A. I. Sanda, Phys. Lett. B **211**, 213 (1988); A. B. Carter and A. I. Sanda, Phys. Rev. Lett. **45**, 952 (1980).
[3] M. Gronau and D. London, Phys. Lett. B **253**, 483 (1991); M. Gronau and D. Wyler, Phys. Lett. B **265**, 172 (1991).
[4] I. Dunietz, Phys. Lett. B **270**, 75 (1991).
[5] D. Atwood, G. Eilam, M. Gronau, and A. Soni, Phys. Lett. B **341**, 372 (1995).
[6] D. Atwood, I. Dunietz, and A. Soni, Phys. Rev. Lett. **78**, 3257 (1997); Phys. Rev. D **63**, 036005 (2001).
[7] A. Giri, Yu. Grossman, A. Soffer, and J. Zupan, Phys. Rev. D **68**, 054018 (2003).
[8] A. Bondar, Proceedings of BINP Special Analysis Meeting on Dalitz Analysis, 2002 (unpublished).
[9] M. Gronau, Phys. Lett. B **557**, 198 (2003).
[10] A. Poluektov *et al.* (Belle Collaboration), Phys. Rev. D **70**, 072003 (2004).
[11] K. Abe *et al.* (Belle Collaboration), hep-ex/0411049.
[12] B. Aubert *et al.* (*BABAR* Collaboration), Phys. Rev. Lett. **95**, 121802 (2005).
[13] B. Aubert *et al.* (*BABAR* Collaboration), hep-ex/0507101.
[14] K. Abe *et al.* (Belle Collaboration), hep-ex/0504013.
[15] A. Abashian *et al.* (Belle Collaboration), Nucl. Instrum. Methods Phys. Res., Sect. A **479**, 117 (2002).
[16] Y. Ushiroda (Belle SVD2 Group), Nucl. Instrum. Methods Phys. Res., Sect. A **511**, 6 (2003).
[17] D. M. Asner *et al.* (CLEO Collaboration), Phys. Rev. D **53**, 1039 (1996).
[18] H. Albrecht *et al.* (ARGUS Collaboration), Phys. Lett. B **241**, 278 (1990).
[19] H. Muramatsu *et al.* (CLEO Collaboration), Phys. Rev. Lett. **89**, 251802 (2002); **90**, 059901(E) (2003).
[20] S. Kopp *et al.* (CLEO Collaboration), Phys. Rev. D **63**, 092001 (2001).
[21] G. J. Gounaris and J. J. Sakurai, Phys. Rev. Lett. **21**, 244 (1968).
[22] E. M. Aitala *et al.* (E791 Collaboration), Phys. Rev. Lett. **86**, 765 (2001).
[23] E. M. Aitala *et al.* (E791 Collaboration), Phys. Rev. Lett. **86**, 770 (2001).
[24] G. J. Feldman and R. D. Cousins, Phys. Rev. D **57**, 3873 (1998).